



UNIVERSITY OF LEEDS

This is a repository copy of *Retrofitting of masonry walls by using a mortar joint technique; experiments and numerical validation*.

White Rose Research Online URL for this paper:
<http://eprints.whiterose.ac.uk/96014/>

Version: Accepted Version

Article:

Wang, C, Forth, JP, Nikitas, N orcid.org/0000-0002-6243-052X et al. (1 more author)
(2016) Retrofitting of masonry walls by using a mortar joint technique; experiments and numerical validation. *Engineering Structures*, 117. pp. 58-70. ISSN 0141-0296

<https://doi.org/10.1016/j.engstruct.2016.03.001>

© 2016, Elsevier. Licensed under the Creative Commons Attribution-NonCommercial-NoDerivatives 4.0 International
<http://creativecommons.org/licenses/by-nc-nd/4.0/>

Reuse

Items deposited in White Rose Research Online are protected by copyright, with all rights reserved unless indicated otherwise. They may be downloaded and/or printed for private study, or other acts as permitted by national copyright laws. The publisher or other rights holders may allow further reproduction and re-use of the full text version. This is indicated by the licence information on the White Rose Research Online record for the item.

Takedown

If you consider content in White Rose Research Online to be in breach of UK law, please notify us by emailing eprints@whiterose.ac.uk including the URL of the record and the reason for the withdrawal request.



eprints@whiterose.ac.uk
<https://eprints.whiterose.ac.uk/>

1. Introduction

Masonry is a composite material made of brick units and mortar that has been used for centuries in building construction. It is in wide usage in seismic-prone areas, especially in the form of infill panels within reinforced concrete (RC) or steel frames. Therein, infills are customarily considered as secondary elements (also referred to as non-structural elements) to the structure and are for simplification not considered in the calculations of seismic capacity. Yet they sustain a large portion of the energy dissipation [1]. As such, their performance can be a decisive factor leading which may lead to a catastrophic structural failure. With this in mind, masonry structures often need to be repaired following earthquake events or enhanced prior to seismic actions in order to ensure that they can perform their highly sought energy absorption and force relieving roles [2]. In the past decades, researchers have implemented different methods to enhance the seismic behaviour of unreinforced masonry walls. These range from the so-called conventional techniques [3] to the latest modern retrofitting techniques [4].

Conventionally, the surface treatment is an approach to improve the masonry wall behaviour. Typical surface treatment includes ferrocement, reinforced plaster and shotcrete, with shotcrete being the most often used method [4]. According to the method, shotcrete overlays are sprayed onto the surface of a masonry wall over a mesh of reinforcing bars. ElGawady et al. [5] carried out tests on retrofitted masonry walls by applying shotcrete. The retrofitting was carried out on either one or both sides, using consistently the same thickness and reinforcement. The test results showed that the ultimate lateral load resistance of the wall can be increased by a factor of approximately 3. However, disadvantages of this method include the considerable time required for the implementation and the adverse impact on the aesthetics of the retrofitted structure.

Grout and epoxy injections are also a broadly used retrofitting approach. The main purpose of the injections is to restore the original integrity of the retrofitted wall and to fill possible behaviour-damaging voids and cracks, which are present in the masonry due to physical and chemical deterioration and/or mechanical actions [3]. The technique was found effective in restoring the initial stiffness and strength of masonry, while its practicality, relatively minimal cost and easiness of implementation have rendered it rather popular among engineers. However, any such approach trivially will be successful only if the mechanical properties together with the physical and chemical attributes of the employed mix end up being compatible with the masonry to be retrofitted [6].

Some of the drawbacks of the quoted conventional methods can be overcome by the Fibre Reinforced Polymer (FRP) reinforcement. Retrofitting of unreinforced masonry walls using FRP can increase the lateral resistance by a factor ranging from 1.1 to over 3 [4]. Alcaino and Santa-Maria [7] presented experimental results from clay brick masonry walls retrofitted with carbon fibre. From the results analysis, it was found that the strength of the walls could increase between 13% and 84%. Also, Mohmood and Ingham [8] conducted a research program in order to investigate the effectiveness of FRP additions as seismic retrofit interventions for in-plane loaded unreinforced masonry walls. The experimental results showed that the shear strength increased up to a factor of 3.25. In general, the retrofitting of masonry walls using FRP material addition has the common advantage of little added mass while mostly producing low disturbance for achieving a relatively high improvement in strength. However, the main drawbacks are the high cost, the high technical skill required for their installation, the affecting of architectural aesthetics and the not so broad experience with these materials particularly relevant to their aging.

To the authors' knowledge, most of the research on the mechanical behaviour of masonry and the retrofitting measures were focused on single-leaf walls, with only very few exemptions expanding on double-leaf or multi-leaf masonry walls. Predicting the behaviour of multiple-leaf masonry walls is a challenging issue, given the influence of a wide range of factors as the mechanical properties of the leaves, their dimensions and the way they are connected to each other. Still, double-leaf walls can be found in many historic structures as well as in modern structures and they have regularly been exposed to considerable earthquakes obviously affecting the holistic structural dynamic performance. Therefore, it feels necessary to also conduct research on such a construction system shedding light on previous gaps in knowledge. Anand and Yalamanchili [9] analysed a composite masonry wall made of block and brick units and tied together by two different in thickness collar joints, 9.5 mm and 51 mm. The composite masonry walls were subjected to both vertical and horizontal loads in a 3D arrangement. From the results analysis, it was found that the collar joint failure is brittle in nature. Pian-Henriques et al. [10] conducted a series of experimental tests on multi-leaf masonry wall panels under a combined shear and compression load with the aim to predict their load carrying capacity and failure mode. The specimens consisted of two external leaves made of stone blocks bonded together with mortar joints while the internal leaf consisted of a mixture of mortar with stone aggregates. A simplified calculation for predicting the compressive strength of composite walls has been presented

good agreement with experimental results obtained. Ramalho et al. [11] modelled the experimental specimens of Pian-Henriques et al. [10] by applying a damage model which was developed to interpret the time evolution of mechanical damage in brittle materials. The models were implemented using the finite element codes ABAQUS and FEAP and comparisons made on the results obtained. The proposed numerical codes were able to capture the different features of the nonlinear mechanical behaviour of multi-leaf walls. However, as perfect bonding was assumed between the adjacent layers during the modelling, some of the numerical results were overestimated. Also, Binda et al. [12] conducted research on multi-leaf masonry walls in order to understand the load-transfer mechanisms between the individual walls although the collar joint which was used for the construction of the walls were much thicker than what is suggested in British Standard 5628-1:2005 [13] (i.e. the space between two parallel single-leaf walls is to not exceed 25mm).

In this paper, a conventional though practical, novel retrofitting approach is introduced. Namely, the traditional method of building a wall parallel to an existing single-leaf wall and bonding the two together using a mortar collar joint is being considered as a possible strengthening and retrofitting technique. The method does not require sophisticated workmanship because of its easy implementation, which further renders it cost-effective.

In general, the application can be divided into two categories: a) the pre-damage enhancement; and b) the post-damage repairing. Earthquake being a specific very interesting catastrophic damage case with great relevance to masonry wall failures is what will be particularly discussed hereafter. For the purpose of the specific project in pre-earthquake enhancement tested walls, the second wall was built parallel to the existing one and bonded with a relatively thin collar joint before the test. For the case of post-earthquake repaired walls, the second wall was attached to the existing one after it had been tested (and as such partially damaged). The collar joint dimensions were kept constant while the damage progressed only to the very early plastic range (i.e. cracking far from collapse). A preliminary parametric study has been conducted to evaluate the performance of the enhancement method using a monotonically increasing quasi-static loading scheme. Notably, the whole study is not only relevant to earthquake engineering, which is a rarity in UK; double-leaf (collar jointed) walls can also be used to improve a structure's lateral stability (e.g. against wind or blast loading) through adding stiffness [14]. Thus, this research broadly aims to generate knowledge and understanding which can be directly applied in a number of structural applications.

On the numerical modelling side, in the past decades, research relevant to masonry walls has been advanced considerably. However, the modelling of a load bearing masonry wall or masonry infill under in-plane combined loading remains difficult primarily due to the complex mechanics developed within the different materials of the wall. A number of different approaches have been implemented to simulate the mechanical behaviour of masonry walls subjected to static or dynamic loading that can act in-plane, out-of-plane or even simultaneously in both planes. The selection of the most appropriate method to use depends on, among other factors, on the structure under analysis; the level of accuracy and simplicity desired; the knowledge of the input properties in the model and the experimental data available; the amount of financial resources; time requirements and the experience of the modeller (Lourenco [15]). Preferably, the approach selected to model masonry should provide the desired information in a reliable manner within an acceptable degree of accuracy and with least cost. According to Lourenco [15], the available strategies for the numerical modelling of masonry structures would fall within one of two categories: a) micro-scale; and b) macro-scale modelling.

In macro-scale modelling, the masonry units and mortar joints are smeared into an averaged continuum. There are no distinctions between the units, the mortar and their interfaces. This model can be applicable when the dimensions of a structure are large enough, compared to the constituent parts, so that a description involving average stresses and strains becomes acceptable [16]. Considerable computational time can be saved by applying this method. However, unconditionally accurate results and fine-detail of the behaviour cannot be captured by the nature of this approach. On the other hand, the micro-scale modelling can be split into the following two approaches: a) simplified micro-modelling; and detailed micro-modelling. In the simplified micro-modelling approach expanded units are modelled as continuous elements while the behaviour of the mortar joints and unit-mortar interface is lumped in discontinuous elements. In the detailed micro-modelling approach both the masonry units and the mortar are discretised and modelled with continuum elements while the unit/mortar interface is represented by discontinuous elements accounting for potential crack or slip planes. Detailed micro-modelling is probably the most accurate tool available today to simulate the real behaviour of masonry as the elastic and inelastic properties of both the units and the mortar can be realistically taken into account. With this method, a suitable constitutive law is introduced in order to reproduce not only the behaviour of the masonry units and mortar, but also their interaction. However, any analysis with this level of refinement requires large computational effort to analyse.

Thus, this method is used mainly to simulate tests on small specimens in order to determine accurately the stress distribution in the masonry materials. The drawback of the large computational effort required by detailed micro-modelling is partially overcome by the simplified micro-modelling strategy. In this case, each joint, consisting of mortar and the two unit-mortar interfaces, is lumped into an “average” interface while the units are slightly expanded in size in order to keep the geometry unchanged. Within this approach, it is possible to consider masonry as a set of elastic blocks bonded together by potential fracture slip lines at the joints. The main methods available for modelling masonry structures using the simplified micro-modelling approach include: a) the discontinuous finite element method; and b) the discrete element method.

When modelling masonry using the discontinuum finite element method, discontinuities are generally introduced using interface elements, for which the constitutive model is in direct relation with the stress vector and the relative displacement vector along the interface (Oliveira [33]). Thus, for an accurate simulation of masonry behaviour, it is essential to obtain a constitutive model for the interface elements which is able to capture realistically the behaviour of masonry and be able to simulate all the failure mechanisms. Page [17] first introduced masonry as a two-phase material, which translates to the bricks taken as linear elastic and the mortar-brick interface taken as inelastic obeying to a simple Mohr-Coulomb failure criterion. Lourenco [18] subsequently introduced a compressive cap to the failure surface in Page’s model. By this crushing of the masonry bricks is also enabled beyond the interfaces, allowing for all possible failure models to be taken into account. Although a micro-scale model needs more computational time, it can let many salient behaviour features to emerge, thus giving a better understanding and predicting insight of the masonry walls’ performance. Al-Chaar and Mehrabi [19] modelled a few RC frames infilled with masonry walls using this method in DIANA. Furthermore, a lot more researchers have applied this method to model masonry structures. (Van Zijl [20], Dolatshahi and Aref [21])

The discrete element method (DEM) is characterized by modelling the materials as an assemblage of distinct blocks or particles interacting along their boundaries. The formulation of the method was proposed initially by Cundall [22] for the study of jointed rock, modelled as an assemblage of rigid blocks. Later this approach was extended to other fields of engineering requiring a detailed study of the contact between blocks or particles such as soil and other granular materials

(Ghaboussi and Barbosa [32]. In the last two decades, the approach was applied successfully to model masonry structures by Lemos [23] and Giamundo et al. [26] in which the collapse modes were typically governed by mechanisms in which the deformability of the blocks plays little or no role. Also, the possibility of frequent changes in the connectivity and the type of contact as well as marked non-linearity induced by the inability of the masonry joints to withstand tension makes DE a suitable method for solving problems involving discontinuities as is the case with low bond strength masonry (Sarhosis & Sheng [24] and Sarhosis et al. [25]).

However, nowadays, in modern FE, the time integration algorithm might be explicit or implicit, the contact size and extent is updated, large or small displacements and rotations can be taken into account, the contact detection algorithms detect new contacts and even self-contact, the contact algorithms are much more sophisticated and accurate than the classical DE contact strategies etc. Therefore, the use of the computational strategy to use is rather a matter of taste provided that the user is experienced.

The development of a computational model based on the discontinuum finite element approach is presented here. Namely the bricks were modelled as rigid elements separated by zero thickness interfaces representing the mortar joints. The interface inelastic properties were simulated using a Mohr-Coulomb failure surface combined with a tension cut-off and a compression cap. The modelling approach when referring to a single-leaf masonry wall panel (i.e. unretrofitted) focused only in two dimensional analyses while for double-leaf masonry walls it is clear that it was necessary to expand in three dimensional one. The model was implemented in the commercial software MIDAS FEA [26] and all analytical results were verified and validated against currently derived experimental outputs.

2. Experimental work

A series of single and double leaf brickwork masonry wall panels were tested in the laboratory. The experimental campaign included four tests on single-leaf and three on double-leaf walls. The experimental observations were primarily focused on static displacement and load capacities clearly supporting a quasi-static rationale for performing any earthquake load related assessments. The in-plane dimensions of each brickwork masonry wall panel tested in the laboratory were 975 mm x 900 mm. All panels were built with stretcher bonded brickwork and rested on a steel base-plate which was constrained by a steel portal.

2.1. Materials

2.1.1. Brick

All the test panels were constructed with UK standard size 215 mm x 102.5 mm x 65 mm Engineering Class B perforated bricks. From the manufacturer's specification, the bricks had average water absorption of 5.6% ($\pm 0.6\%$), porosity equal to 25%, density of approximately 1885kg/m³ and compressive strength of the order of 35 N/mm². A series of small scale tests to investigate the modulus of elasticity of bricks have been performed according to BS 3921:1985 [27] and BS EN772-1:2011[28]. In total, ten samples were tested and the elastic modulus of the bricks was found to be equal to 19.9 kN/mm².

2.1.2. Mortar

There were two different types of mortar used in the experiments. These are: a) Type S; and b) Type N. Type S had mix proportions of Ordinary Portland Cement (OPC) : lime : sand equal to 1:1/2:4 1/2. The compressive strength for 100 mm cubes cured in a fog room with 99% relative humidity and 21 °C temperature was 12.7 MPa (± 1.2 MPa) (based on eight tests). Type N had mix proportions of Ordinary Portland Cement (OPC) : lime : sand equal to 1:1:6. The compressive strength for 100 mm cubes cured in a fog room with relative humidity 99% and temperature 21 °C was 6.7 MPa (± 0.4 MPa) (based on eight tests). All mortar compressive strength tests were undertaken as per BS EN 1015-11:1999 [29]. The mortar joints were all nominally 10 mm thick.

2.2. Panels' tests arrangements and procedure

Each wall panel was tested by applying an external load on the top-left hand corner. The load was applied to each panel using a hydraulic ram and was distributed through a thick steel spreader plate which was embedded in mortar on the surface of the brickwork. The steel plates were spanning over the top three courses in the vertical direction and over one brick length horizontally. There was a 10 mm gap initially, which then increased to 20mm, between the unloaded side of the panel and the portal frame column in order to provide clearance for horizontal displacements. For the first three

courses, starting from the base, this gap was filled with mortar to restrict any horizontal movement allowance of the wall.

A horizontal load was applied to each wall incrementally (2 kN/min) until the panel could no longer carry the applied load. Among others, the scope of the test rig was to potentially simulate the RC frame restraint as experienced by a real infill wall. Therefore, a vertical load cell was also used to suppress the vertical uplift of the restrained leaf, mimicking the interaction with an RC frame. Initially the vertical load was set to 20 kN (and subsequently adequately increased with target to limit any base rotation). Furthermore, a LVDT was set up on the top hand corner of the panel. At each load increment, the LVDT's readings were monitored for signs of continued gradual increase in deflection under constant load. This re-distribution of stress was particularly noticeable as cracks developed and propagated through each panel. During the test, surface cracking was inspected visually. Typically the first visible cracks were of the order of 0.2mm wide. The test rig for the single-leaf wall is shown in Figure 1.

A second series of tests was subsequently carried out for all double-leaf walls on an updated apparatus (Figure 2). The second leaf was built parallel to the existing one and was 'tied' to it using a 10mm thick collar joint. The material of the collar joint was exactly the same to the mortar joint used for the construction of the second leaf wall. Mortar was successively filling up to the bricks' top and the collar joint after constructing each new layer of bricks. Therefore, it can be simply assumed that any holes in the bricks and collar joint between the two walls were fully filled with mortar. There was no surface treatment applied on the walls. Also, the new panel was not restricted in any way by the portal frame, which meant that it could move freely throughout its length along its in-plane axis. The load was solely applied to the initial panel which was restricted by the portal frame, while the loading setup was exactly the same to the single-leaf case. Thus, there was no direct loading applied to the second leaf wall; the only load sustained was transferred by some shear transfer mechanism from the initial panel.

For the double-leaf walls, there was a further division into two categories relevant to their damage stage. These will be quoted as "*pre-earthquake*" and "*post-earthquake*". In the pre-earthquake case, the second-leaf wall was attached to the first leaf wall before it even got any load. Ideally, any practical retrofit action is performed much later than the initial structural installation. Still at this level a sensible problem reduction approach needs to first address the concurrent wall installation

as this being the simplest possible answer to the complexity of the aging process. As a matter of fact this rationale excludes the parameter of differential aging from the multivariate problem in-hand. In the post-earthquake case, the second leaf was attached to the first one only after the latter had nominally failed making it essentially a means of repair. In all cases, walls had been cured for 14 days under a polythene sheet before being loaded. To this testing rule there was only one exception. The referred to as wall W6 (a single-leaf wall) was cured for an extended period of 42 days before being tested in order to have some indication of the curing impact and a baseline for the efficacy of any later remediation. The preparatory single-leaf test was interrupted when initial fine cracking occurred. Subsequently it did not get any crack repair, since these were of hairline nature, and got retrofitted by “attaching” a second wall to it using the previously discussed mortar collar joint technique (becoming then Wall 7). A summary of the full test configurations studied, indicating the adopted tests’ naming conventions for any later reference is provided in Table 1.

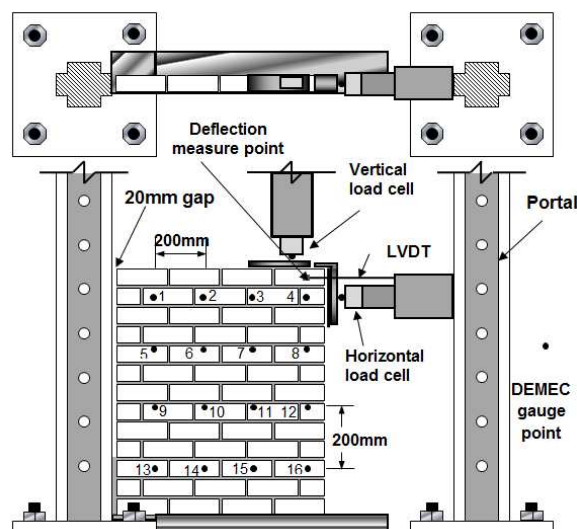


Figure 1. Testing rig of single-leaf panel

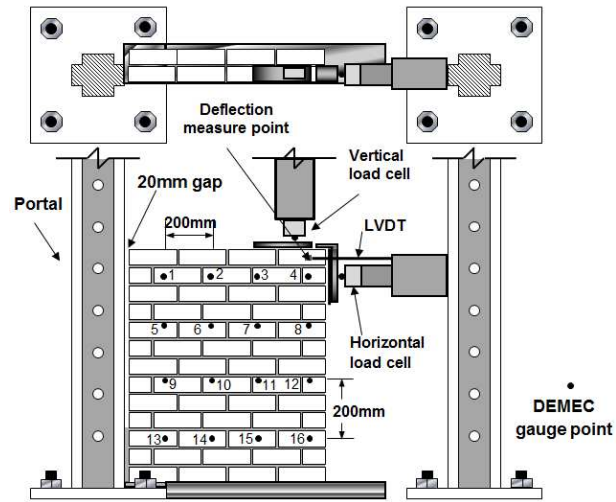


Figure 2. Testing rig of double-leaf panel

Table 1. Summary of test results

Wall name	Wall type	Mortar type	Days cured	Case
W1	Single-leaf	S	14	-
W2	Single-leaf	S	14	-
W3	Single-leaf	N	14	-
W4	Double-leaf	N	14	Pre-earthquake
W5	Double-leaf	N	14	Pre-earthquake
W6	Single-leaf	N	42	-
W7	Double-leaf	N	14	Post-earthquake

3. Experimental results

3.1. Failure patterns; an initial qualitative assessment

3.1.1. Single-leaf walls

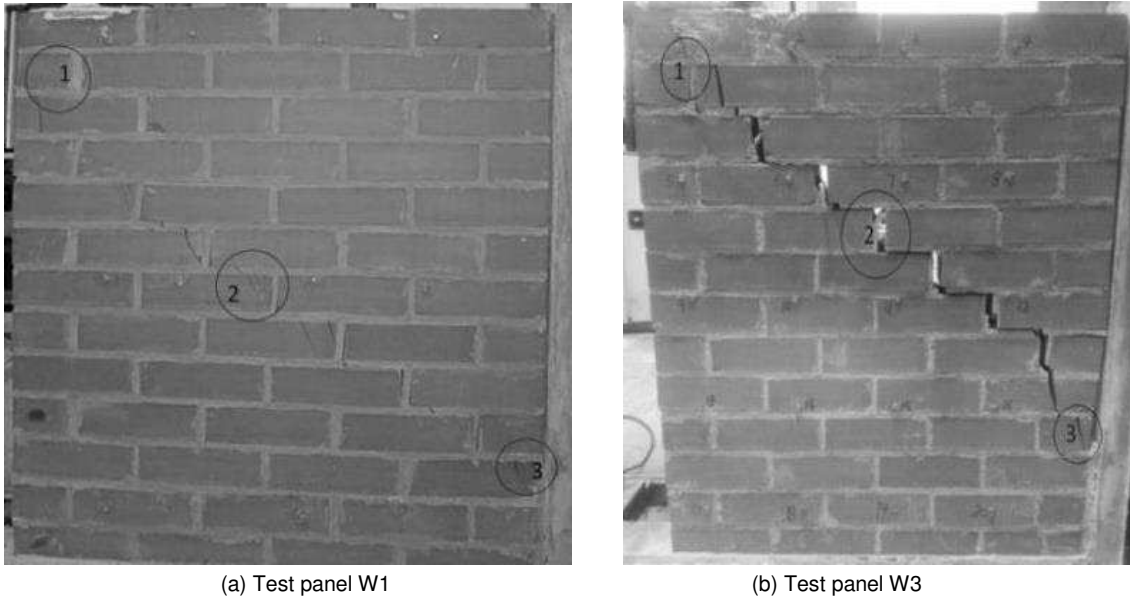


Figure 3. Failure pattern of single-leaf walls

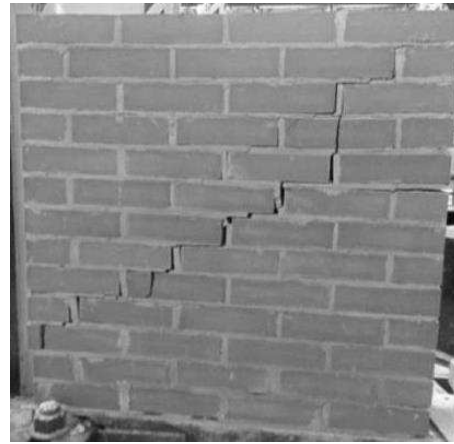
Figure 3 shows the failure pattern of the single-leaf masonry wall panels W1 and W3. Very similar failure patterns were observed for the other single-leaf masonry walls (W2 and W6). According to the failure patterns shown in Figure 3, the failure mode of a single-leaf wall can be described by a major diagonal crack. Before this diagonal crack developed, some small, hairline shear cracks appeared along the bed joint length. Further, with increasing horizontal load, the top corner of the wall (indicated as area 1 in Figure 3) began to crush and cracks started propagating from that region down to the base of the wall. Stresses kept increasing with applied load and once the strength of the masonry was exceeded the failure occurred in the form of the earlier quoted diagonal crack spanning widely from area 1 to area 3, following a staircase path along the mortar interfaces. This typical mechanical behaviour of a masonry wall under lateral load can also be seen in the work of Vermeltoort et al. [30]. The wall point at the top of the edge gap-filling mortar in area 3 is clearly a point of rotation and as expected no local extensive crushing of the masonry was observed below this region. In this experimental study, the occurrence of the diagonal crack signified the end of the testing. However, in practice a masonry panel loaded in-plane within a frame will become locked in and continue resisting the panel deformation even after the diagonal cracks are formed; the most notable aspect of such a scenario is the potential for additional energy dissipation (Mehrabi et al. [1]) allowed within the restrained sliding of the damaged interfaces. These tests do not consider any load cycling or dynamic effect that is critical for assessing holistically along these lines the masonry performance.

Still they constitute an insightful first attempt to explain and comprehend the up-to failure performance of the masonry wall.

3.1.2. Double-leaf walls



(a) Front side (loaded wall)



(b) Back side (parallel wall)

Figure 4. Failure pattern of double-leaf wall W5



(a) Front side (loaded wall)



(b) Back side (parallel wall)

Figure 5. Failure pattern of the double-leaf wall W7

3.1.2a Pre-earthquake test

Figure 4 shows the failure mode of the wall panel W5. From Figure 4, it is clear that the pre-earthquake double-leaf walls failed by diagonal cracking, similar to the single-leaf wall case. However, at this instance walls had more cracks than their single-leaf counterpart prior to the formation of the decisive diagonal crack that signified the ultimate failure; this is a sign that for the double-leaf walls, ductility (i.e. extend of plastic deformation) had improved through the presence of a second leaf. In terms of the failure process, first, some small hairline cracks appeared along the bed joints on both leaves; similar to the single-leaf wall previously. Note that the cracks in the second leaf appeared later

than the ones on the first leaf. Further, in all cases and at all times the cracks of the second leaf were less compared to the cracks of the first leaf. Thus, it becomes apparent that the stress transfer between the two leaves was effective throughout the different loading stages as initially envisaged. Namely, the load is applied directly to the first wall and distributed to the second wall consistently via the collar-joint. Therefore, although the two leaves are joined and the width of the loaded area is effectively close to double the initial, the real stress is not distributed evenly, being concentrated at the top corner of the first wall and “flowing” inhomogeneously into the second wall. The uneven distribution of the stresses between the two walls is also influenced by the boundary conditions imposed. The second leaf is not restrained by the gap-filling mortar and therefore is becoming less stiff. The two walls are bonded together acting in a way as a composite construction (Figure 6a).

3.1.2b Post-earthquake test

Figure 5 shows the failure mode as observed in the double leaf brickwork masonry wall panel W7. It can be seen that the first leaf of the post-damaged masonry wall panel behaved in a similar manner to the single-leaf masonry wall panels tested previously where failure was governed by a wide diagonal crack. This is obviously affected strongly by the preloading and incipient damage induced to the wall. However, the second wall behaved quite differently to what was seen before. The actual failure for this case was established by a horizontal shear crack, initiated by the failure of the collar joint. The collar joint actually detached itself from the first wall whilst remaining connected to the second wall (Figure 6b). Therefore, the collar joint did not manage to sustain the integrity of the construction throughout the experiment. The composite masonry wall constituents nearly work individually after the first wall debonded from the second. The cracking pattern succession observed in the first wall was also very different to that seen in the second wall. In the front side of the wall panel W7 diagonal cracks passed through the mortar joints and crossed the bricks. However, in the back side of the wall panel W7, only a small sliding and stepped crack appeared at the bottom of the wall. The localization of this sliding and stepped crack must intuitively follow a weakest link path through the mortar joints.



(a) Top side of W5



(b) Top side of W7

Figure 6. Failure patten of the collar joint

3.2. Failure load and deflection

Table 2. Failure load and deflection of all tests

Test No.	Wall type	Horizontal load (kN)	Displacement at yield point (mm)	Maximum displacement (mm)	Mortar compressive strength (MPa)	Case
W1	Single-leaf	58	9.7	13.1	12.7	-
W2	Single-leaf	64	10.1	11.2	15.3	-
W3	Single-leaf	70	8.2	20.0	6.7	-
W4	Double-leaf	91	10.1	11.4	6.3	Pre-earthquake
W5	Double-leaf	93	10.3	12.6	6.6	Pre-earthquake
W6	Single-leaf	75	9.03	9.03	8.1	-
W7	Double-leaf	77	8.8	17.6	7.1	Post-earthquake

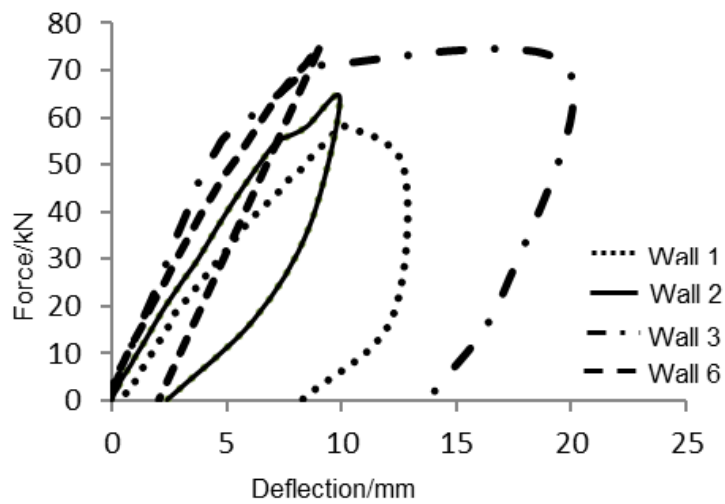


Figure 7. Load-Deflection relationship of single-leaf walls

The ultimate failure loads along with critical deflection parameters for all tests are summarised in Table 2. The load against deflection curves for the ensemble of single-leaf walls is shown in Figure 7. The stiffness of wall W1 is very similar to, although slightly lower than that of W2. More importantly some extensive capability for plastic deformation is observed in wall W1 while this was not the case for W2. W1 could deform even more and its full plastic range was not pursued since the limitation of the apparatus clearance was reached (this was increased only thereafter). Such experimental deviations are expected in similar masonry constructions, yet this seems to be quite a substantial difference that should probably get attributed to a substantial material deviation that wasn't identify. When referring to the different mortar type wall W3 (i.e. Type N, see Table 1) all strength and deformation capacity variables increased consistently and substantially.

The testing of wall W6 was stopped when it was nominally assumed to have yielded; this state was taken at the point when initial 'fine' cracking appeared and the horizontal load-deflection relation started deviating increasingly from the initial elastic region. At that point W6 was unloaded and its damaged stage was considered the base for the later post-damage retrofitting study. Figure 7 reveals that there was no considerable post-peak load behaviour captured for W6 as intended (see elastic recovery). The stiffness of wall W6 was evidently greater than that of W1 and W2. Although this can be attributed to the increased curing time (i.e. compared to W1 and W2, W6 was cured for 42 days instead of 14 days) this increased stiffness being also apparent in the case of W3 seems mainly a product of the different mortar type. However, the stiffness of the W6 is lower than that of W3, further implying the small effect of additional curing times beyond a certain duration.

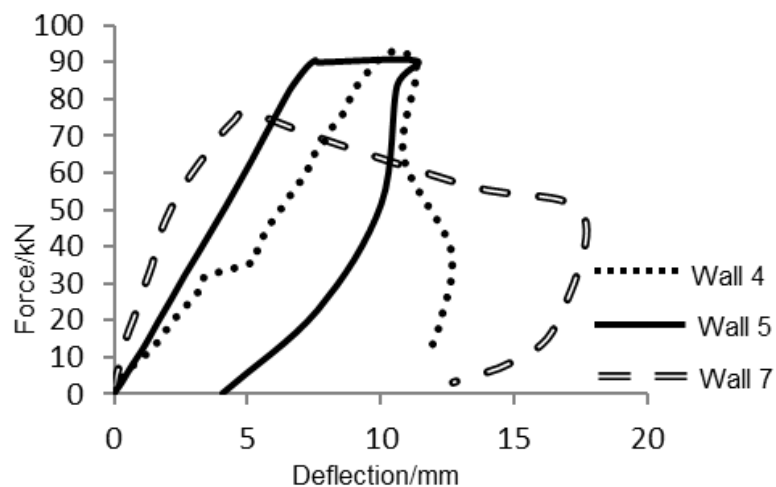


Figure 8. Load-Deflection relationship the of double-leaf walls

Figure 8 illustrates the horizontal load-deflection behaviour for all the collar-jointed masonry walls. Walls W4 and W5 (pre-earthquake method) exhibited a much higher failure load (91 kN and 93 kN, respectively) than any of the single leaf walls, which failed at loads ranging between 58 kN to 70 kN. Although W4 and W5 have similar failure loads, yet their ultimate deflection differs. This is an artificial output with the measurement of W4 encompassing a slippage contribution without which the displacement behaviour becomes quite alike to W5 rendering any remaining difference falling within the acceptable experimental deviation bands. Interestingly, wall W7 (the post-earthquake retrofit wall), although only achieving a failure load more in-line with the single-leaf walls (around 80 kN) going approximately only halfway through the capability gains of the pre-earthquake retrofit method, exhibits sustained ductility with much more gradual/reduced softening.

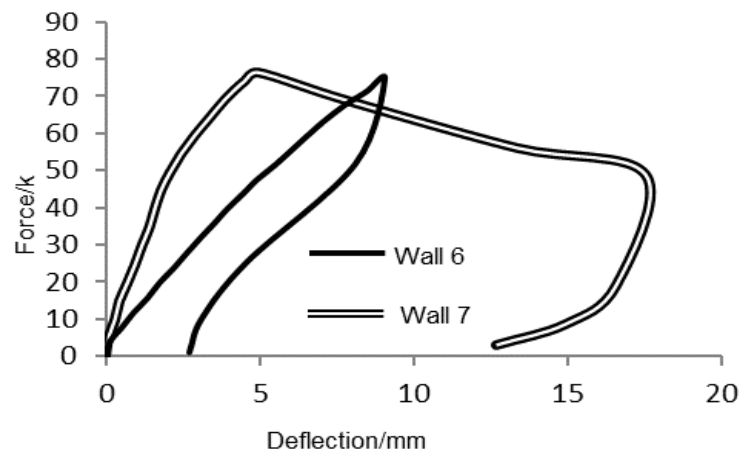


Figure 9. Load-Deflection relationship of post-earthquake strengthening

Figure 9 presents the load against deflection curves for walls W6 and W7. It can be seen that although the failure load of the repaired and strengthened double-leaf wall (W7) was not substantially increased, the initial stiffness has been improved significantly; it actually reached a value almost twice the single-leaf one (W6). For the repaired double-leaf wall (W7), a significant amount of ductility was observed, as previously quoted, yet, this is not strictly comparable to the single leaf damaged variant. This is due to the fact that testing of W6 stopped when only initial cracks appeared on its body naturally yielding that the amount of ductility represented in Figure 9 is not indicative of its full capacity.

4. Development of the computational models for masonry

The development of computational models to simulate the mechanical behaviour of the brickwork masonry wall panels tested in the laboratory is presented hereafter. The devised models were based on the micro-scale modelling approach (Lourenco [15]) and were developed using the commercial software MIDAS FEA [18]. For the development of the numerical model, the mortar joints were lumped into a zero-thickness interface while the dimensions of the brick units were expanded to keep the geometry of the given masonry structure unchanged. In addition, vertical predefined cracks were assigned to the middle of each brick element (Figure 10). This is due to the fact that in masonry structures, as also evidenced in the current experimental failure patterns, most of the propagating cracks beyond being located in the mortar they also develop across the bricks [24, 25].

For the 2D models, practiced in the case of single leaf walls, the brick units were represented by eight-noded plane stress continuum elements, while the brick-mortar interfaces were represented by six-noded line interface elements. For the 3D models relevant to collar jointed walls, the bricks were represented by eight-node hexahedron solid elements while surface interface elements were used to analyse the interface behaviour between the solid brick elements. Bricks were assumed to behave in a purely elastic manner while the joint interfaces were simulated using a Mohr-Coulomb failure surface combined with a tension cut-off and a compression cap. For all the cases, the size of the mesh was kept at less than 50 mm.

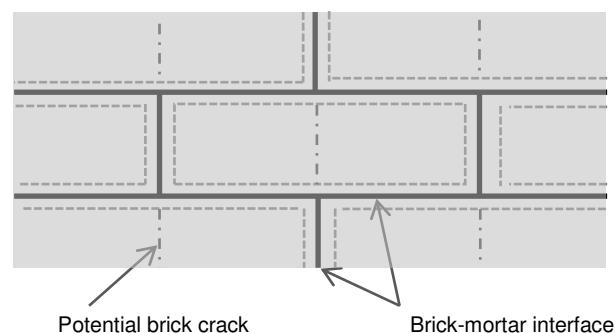


Figure 10. Micro-modelling strategy for masonry (after Lourenco [15])

4.1 Single-leaf walls; comparison to experiments

For the 2D geometrical models representing the single-leaf brickwork wall panels tested in the laboratory the consideration of the 10mm thick mortar joints was taken by increasing by 5mm in each

relevant face direction the brick size in order to give a typical MIDAS block size of 225mm x 102.5mm x 75mm (see Figures 10 and 11 to identify the model geometry).

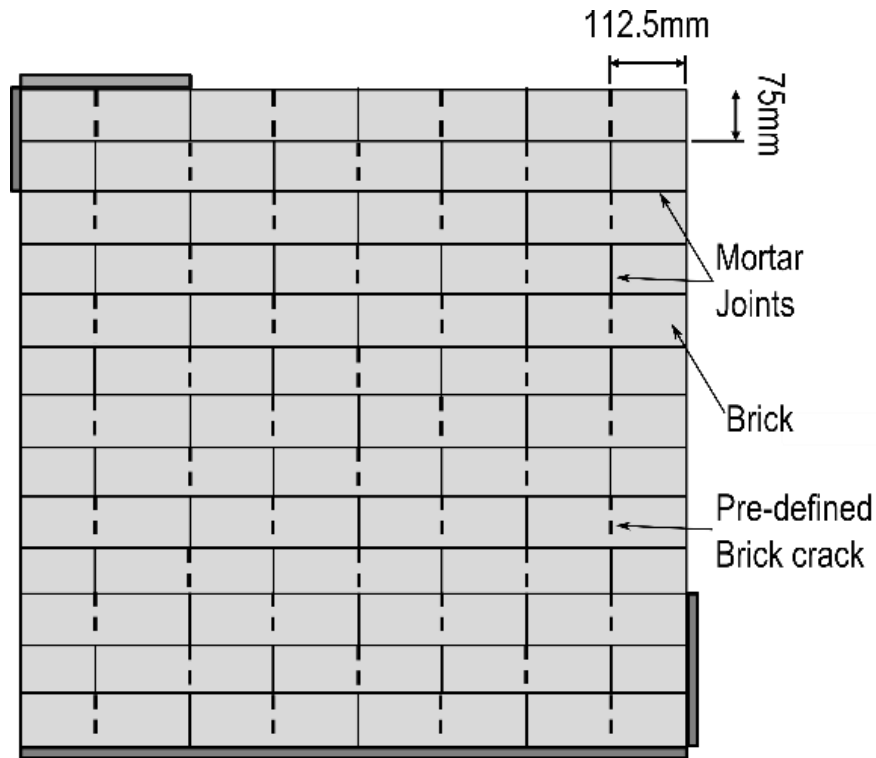


Figure 11. The validation 2D model geometry in MIDAS FEA

4.1.1 Material parameters

For brick-mortar interfaces, the normal stiffness (k_n) and shear stiffness (k_s) are very difficult to obtain. Therefore, they are both assumed based on previous literature values (see Lourenco [15], [18]). An extensive study on the mechanical behaviour of brick-mortar has been conducted by Van der Pluijm [31]. Van der Pluijm found that the bond strength f_t varies between 0.3 to 0.9 N/mm² and the mode I fracture energy G_f^I , from 0.005 to 0.02 Nmm/mm². BS 5628: 2005 [13] gives design values for cohesion C ranging from 0.35 to 1.75 N/mm² and $\tan \theta$ for friction equal to 0.6. Van der Pluijm found that the Mode II fracture energy G_f^{II} ranges from 0.01 to 0.25 Nmm/mm² while the initial cohesion value ranges from 0.1 to 1.8 N/mm². If only one of the fracture mode energy is given, then the other one can be obtained simply as $G_f^{II} = 10G_f^I$. In addition, Van der Pluijm found that the tangent of the initial internal friction angle $\tan \theta_0$ ranges from 0.7 to 1.2 for different unit/mortar combinations. The tangent of the residual internal friction angle $\tan \theta_r$ was approximately constant

and equal to 0.75. The average value for dilatancy angle $\tan \varphi$ ranges from 0.2 to 0.7 depending on the roughness of the brick surface for low confining pressure. Based on the above background and some preliminary testing attempts all the material values required for the implementation of the single-leaf wall in MIDAS FEA are shown in Tables 3 and 4.

Table 3. Properties of the brick masonry units.

Variable	Value
Unit Weight \bar{d} [kg/m ³]	1885
Young Modulus \bar{E} [kN/mm ²]	19.9
Poisson's Ratio ν	0.15

Table 4. Properties of interfaces

Variable	Brick-mortar interface	Brick interface representing potential vertical crack
Normal stiffness k_n (N/mm ³)	13	1000
Normal stiffness k_s (N/mm ³)	5.3	1000
Tensile strength f_t (N/mm ²)	0.4	2
Tensile fracture energy G_f^I (Nmm/mm ²)	0.022	0.08
Cohesion C (N/mm ²)	0.56	-
Friction coefficient $\tan \theta$	0.75	-
Dilatancy coefficient $\tan \varphi$	0.56	-
Shear fracture energy G_f^{II} (Nmm/mm ²)	0.175	-
Compressive strength f_c (N/mm ²)	8.5	-
Compressive fracture energy G_c (Nmm/mm ²)	5.0	-
Compressive plastic strain at f_c	0.093	-

4.1.2 Modelling results

Figure 11 shows a qualitative comparison of the failure patterns developed in the numerical and experimental tests. The relevant horizontal load-deflection curves for the wall W3 are presented in Figure 12. In Figure 12 it can be seen that the computational model is capable to capture with sufficient accuracy the failure mode. Further, Figure 13 compares the experimental against the numerical load against displacement curves. In Figure 13, the computational model is able to capture the stiffness of the wall obtained experimentally for the elastic and incipient plastic deformation regions. This translates to a load reaching above 55kN. At that point, some deviation starts developing with the numerical model showing some first cracking signs which still do not affect

majorly the stiffness which continues unreduced towards reaching a maximum load value in close proximity to the experimental observations. The wall showed a distinctively different behaviour regarding the plastic region with the numerical analogue showing its collapse soon after reaching the ultimate load whereas the experimental case presented increased ductility. Very interestingly shape-wise this looks like the difference between wall panels W1 and W2 observed experimentally earlier. Such a difference yet may well be caused by the difference with which the frame restraint was numerically realised. Relevant to this probably one should note the correct cracking patterns that extend accurately beyond the mortar through bricks in all cases.

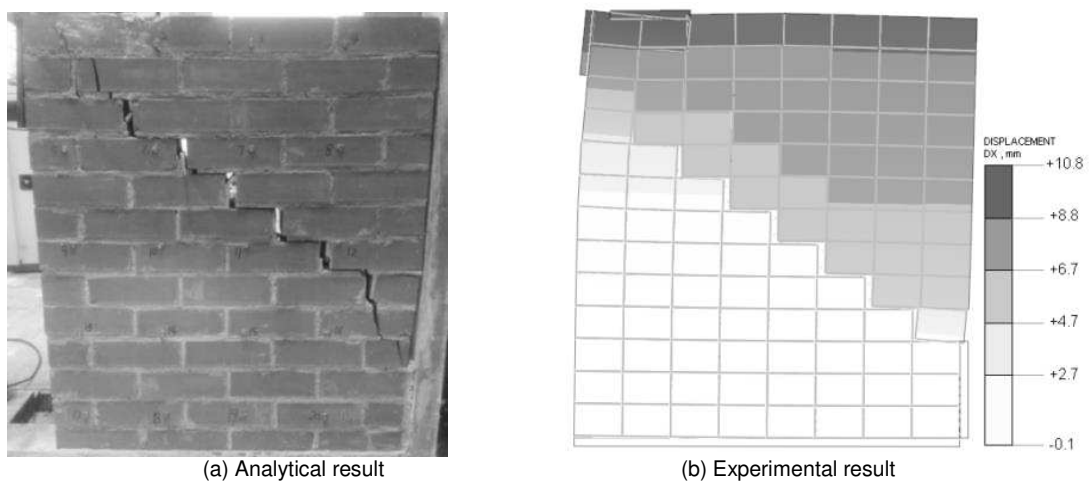


Figure 12. Failure pattern of single-leaf masonry wall W3

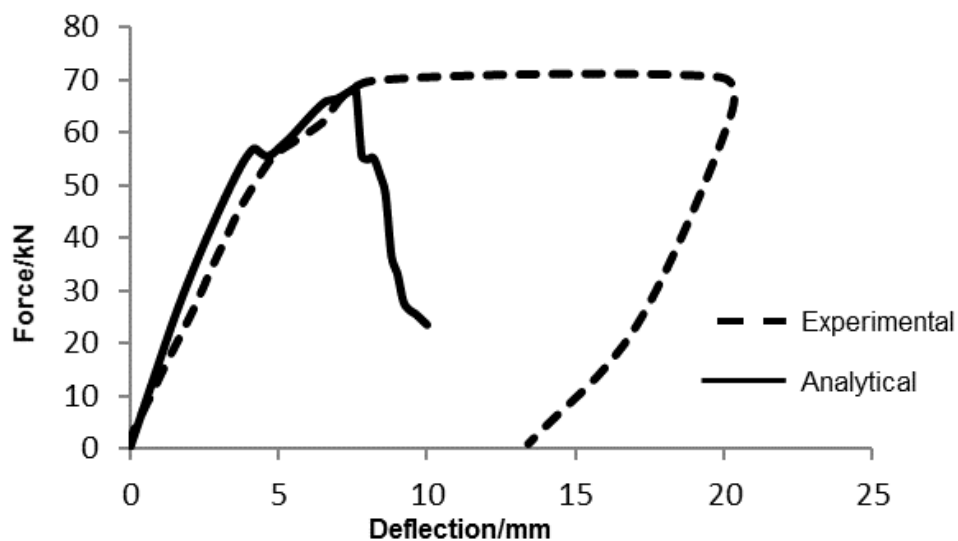


Figure 13. Load-deflection of wall W3

4.2 Double-leaf walls (pre-earthquake); comparison to experiments

3D geometrical models representing the double leaf brickwork panels connected with collar joint were created again in MIDAS FEA (Figure 14) using similar to the 2D previous assumptions (e.g. a potential crack was again placed in the middle part of the bricks). Trivially the behaviour of the collar joint is decisive for the overall behaviour of the wall. Likewise the mortar joint, the collar joint was smeared into an interfacial element of zero thickness.

4.2.1 Material parameters

Since the two merged walls have been constructed at the same time and were cured under identical conditions, their material properties would be the same. In this circumstance, the behaviour of the interfaces pertaining to the two leaves can be modelled with the same interface property as the single-leaf wall shown in the above section (see Table 3). However, the material property of the collar joint is not known a priori. As the mortar used in the collar joint is the same to that used on the bed and head joints, the property can be assumed similarly. However, unlike bed/head joints, the collar joint was not compressed by the external vertical or horizontal load, resulting in the normal/shear stiffness and cohesion to be relatively smaller. The additional material parameters artificially reduced to comply with this rationale are presented in Table 5.

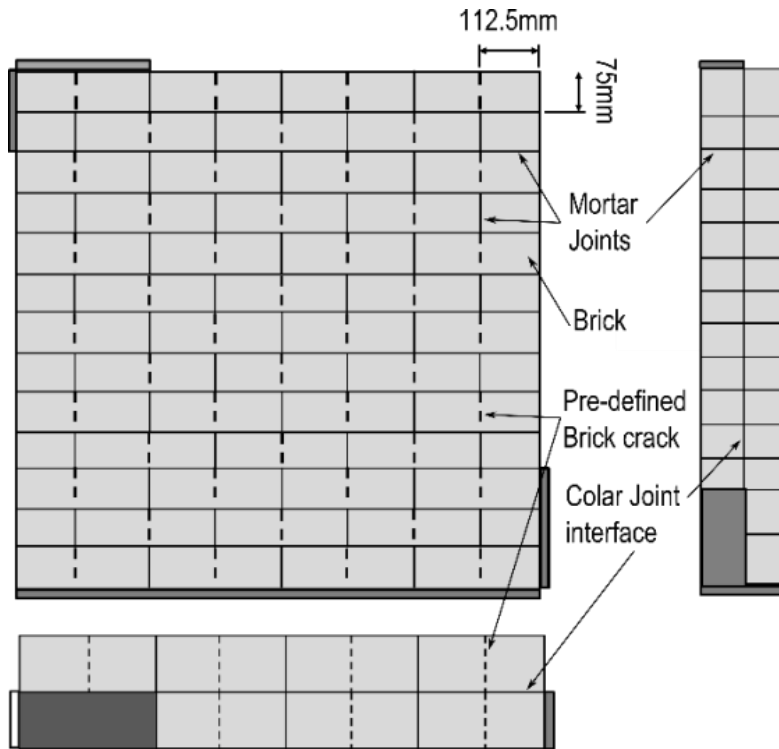


Figure 14. The validation 3D model in MIDAS FEA

Table 5. Properties of different interfaces

Variable	Collar joint
Normal stiffness k_n (N/mm ³)	9
Shear stiffness k_s (N/mm ³)	3.6
Tensile strength f_t (N/mm ²)	0.22
Tensile fracture energy G_f^I (Nmm/mm ²)	0.018
Cohesion C (N/mm ²)	0.30
Friction coefficient $\tan \theta$	0.75
Dilatancy coefficient $\tan \varphi$	0.56
Shear fracture energy G_f^{II} (Nmm/mm ²)	0.17
Compressive strength f_c (N/mm ²)	8.5
Compressive fracture energy G_c (Nmm/mm ²)	5.0
Compressive plastic strain at f_c	0.093

4.2.2 Modelling results

Figures 15 and 16 show the qualitative comparison of failure patterns developed in both the numerical and experimental scenarios. Macroscopically the cracks seem to have occurred in similar positions and formations on both sides. Still there is some difference when one observes in detail the

developed cracks (extend of cracks, passing through bricks etc.). Such differences most probably originate due to local weak zones in the built wall. Still the match is acceptable indicating the good approximation in modelling the collar joint and the inherent variability in masonry materials. In Figure 17, the relevant load against deflection curves for wall panel W4, in both the analytical and experimental cases, showed really close behaviour concerning all the critical parameters (i.e. maximum load, failure deflection and stiffness). In the numerical case, when comparing to the single leaf wall studied before the developed plasticity substantially increased, yet it still couldn't reach to the levels observed during the experiment.

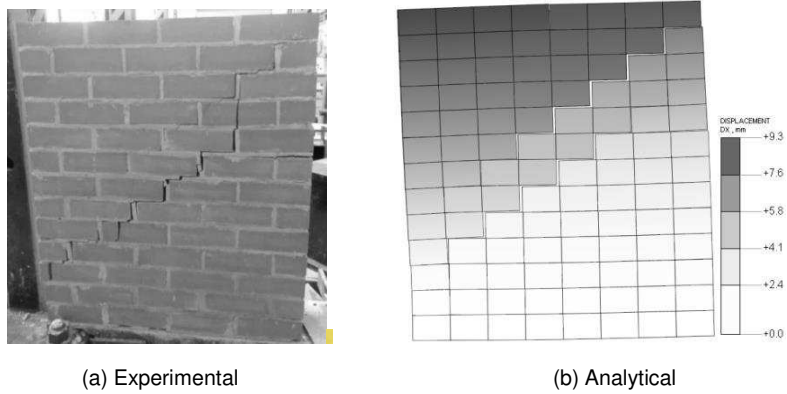


Figure 15. Failure pattern of double-leaf masonry wall 4 on the back side

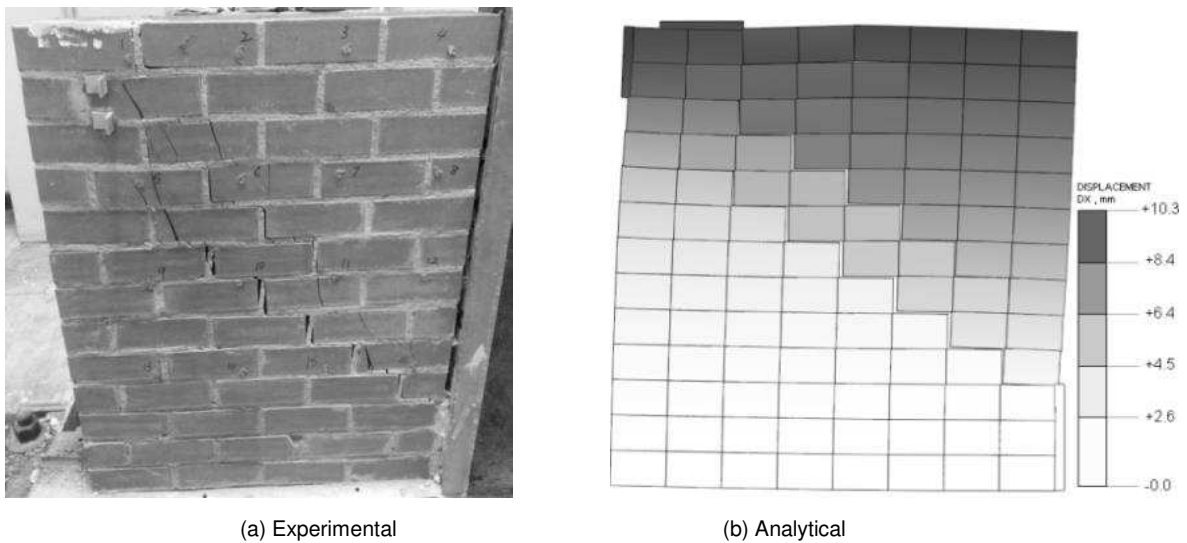


Figure 16. Failure pattern of double-leaf masonry wall 4 on the front side

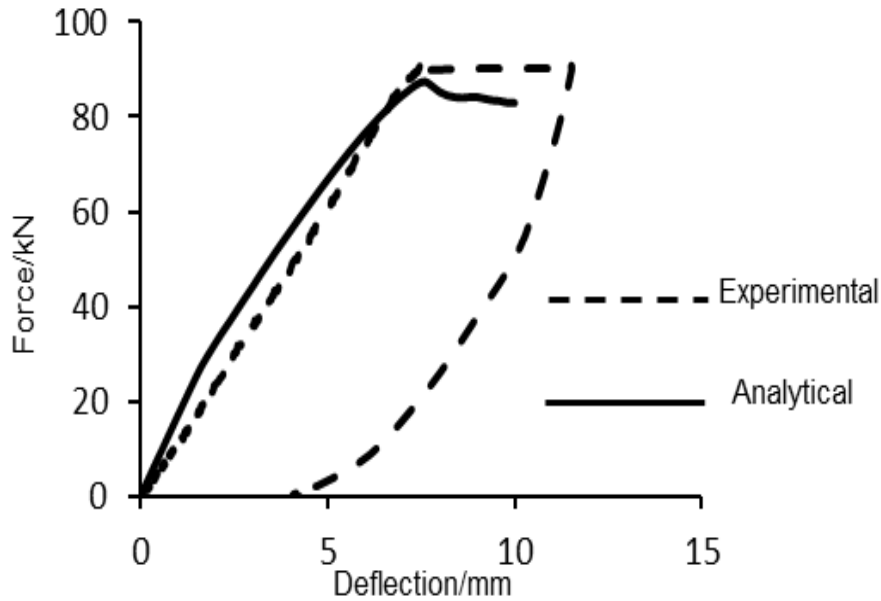


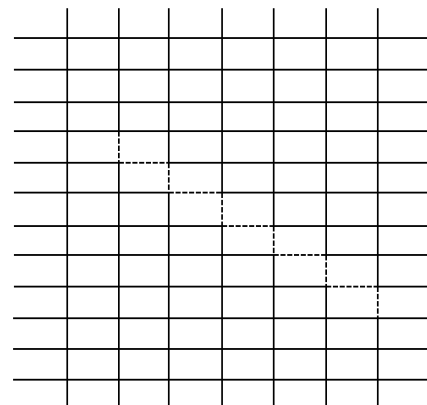
Figure 17. Load-deflection curve of Wall 4

4.3 Double-leaf walls (post-earthquake); comparison to experiments

For the masonry wall W7 the damage introduction results to some interesting modelling idiosyncrasies. The existence of some initial minute cracks in the first wall need to also be approximated correctly if an accurate behaviour is to surface from the modelling attempt. Based on the experimental observations, a grid of existing cracks was pre-defined. This is represented by dashed lines in Figure 18, showing the geometry of the numerical implementation of the wall. In this model, the cracks were assumed to not have any interaction (though there might be some residual friction within them). The boundary conditions were envisaged to be identical to the previous double-leaf wall setup (i.e. pre-earthquake).



Figure 18. (a)Cracks in experimental results



(b)pre-defined cracks in finite element modelling

4.2.3 Materials' parameters

In this case with the first wall having been cured for 42 days and the second having been cured for only 14 days, the two leaves had to be modelled differently. Thus, the brick-mortar interface for the two walls acquired different parameters. To this one should further note the need for different modelling of the collar-joint that was of particular significance in this study. The first leaf owing to its additional curing time when compared to the second leaf was considered having more strength. The joint properties within the second leaf were taken identical to the previous single-leaf walls. Contrary to the previous approach where the collar joint has been uniformly smeared out now it wasn't due to the fact that the interface between the first leaf and the collar joint (interface 1) is different to the one between the second leaf and the collar joint (interface 2) (see Figure 19). Namely the collar joint being built at the same time with the second leaf, was considered with properties identical to the pre-earthquake collar joint case, while the connection with the first leaf was considered minutely weaker. Based on these assumptions, the now extended list of material parameters are given in Table 6.

Table 6. Properties of the zero thick ness interfaces (to read in conjunction with Figure 19)

Variable	1 st leaf mortar	2 nd leaf mortar	Collar joint interface 1	Collar joint interface 2
Normal stiffness k_n (N/mm ³)	15	13	8.5	9
Shear stiffness k_s (N/mm ³)	6.0	5.3	3.5	3.6
Tensile strength f_t (N/mm ²)	0.45	0.4	0.22	0.22
Tensile fracture energy G_f^I (Nmm/mm ²)	0.022	0.022	0.018	0.018
Cohesion C (N/mm ²)	0.56	0.56	0.3	0.3
Friction coefficient $\tan \theta$	0.75	0.75	0.75	0.75
Dilatancy coefficient $\tan \phi$	0.56	0.56	0.56	0.56
Shear fracture energy G_f^{II} (Nmm/mm ²)	0.175	0.175	0.2	0.17
Compressive strength f_c (N/mm ²)	8.5	8.5	8.5	8.5
Compressive fracture energy G_c (Nmm/mm ²)	5.0	5.0	5.0	5
Compressive plastic strain at f_c	0.093	0.093	0.093	0.093

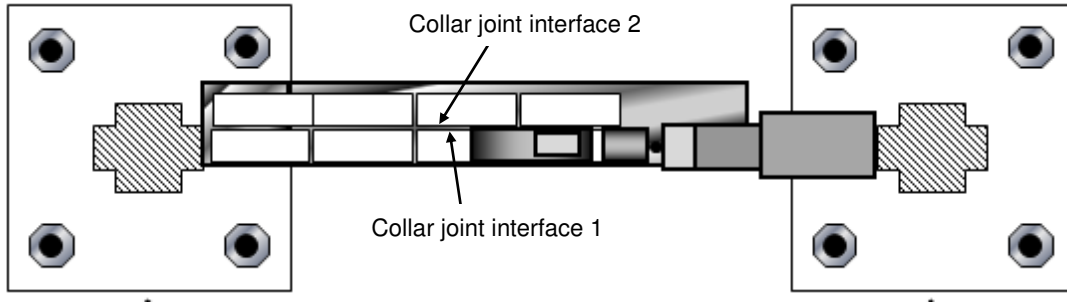


Figure 19. Plan view of the double leaf brickwork masonry wall illustrating the collar joint interface 1 and 2 (To read in conjunction with Figure 2).

4.2.4 Modelling results

The failure patterns for the retrofitted wall in all cases are shown in Figures 20 and 21. Again macroscopically the match is quite accurate between model and numerical prediction, particularly when considering the somewhat approximative character of the interface properties adopted. The overall extend of the cracks and their distributions in the different leaves are in good agreement while salient features such as the exact crack position and length differ. The newly built wall side, although being considered perfectly bonded to the initial side it could not actually relieve it considerably from stresses. Without carrying much load, as evidenced from its minor damage, it followed the whole wall's failure being ultimately quite intact with minimal cracking. As the front side was pre-damaged and also carried most of the loading during the test in the end it got completely damaged, by forming two main step-like diagonal cracks. This failure mode was well captured numerically. Furthermore, there appeared to be more cracks compared with the pre-earthquake scenario. Figure 22 shows the horizontal load-deflection relationship of W7. Therein, the analytical modelling shows an extensive drop in load after yielding and a much reduced plastic zone as also seen earlier. Still the ultimate load and stiffness, which is substantially improved compared to the single leaf case, are well predicted.

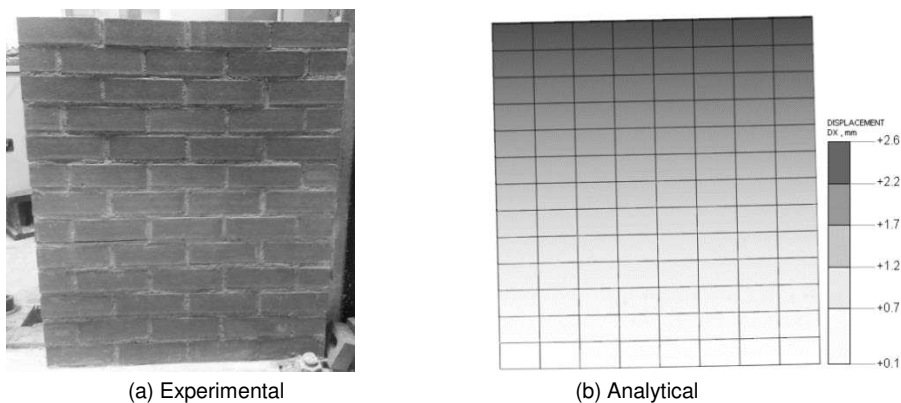


Figure 20. Failure pattern of double-leaf masonry wall on the back side of W7

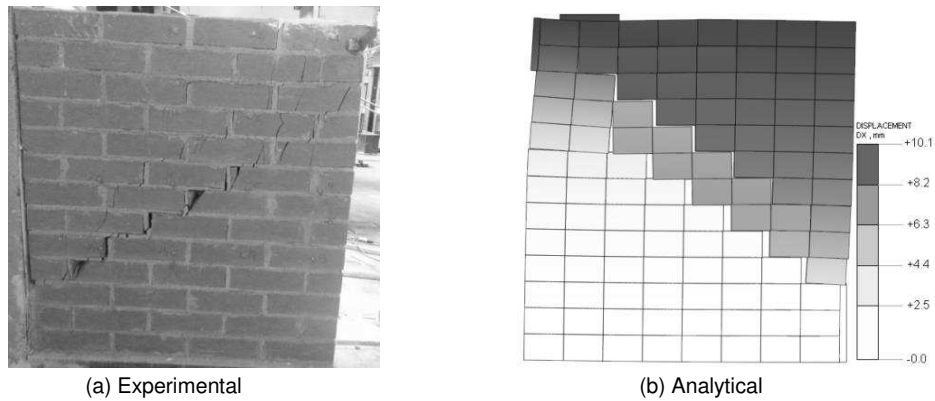


Figure 21. Failure pattern of double-leaf masonry wall on the front side of W7

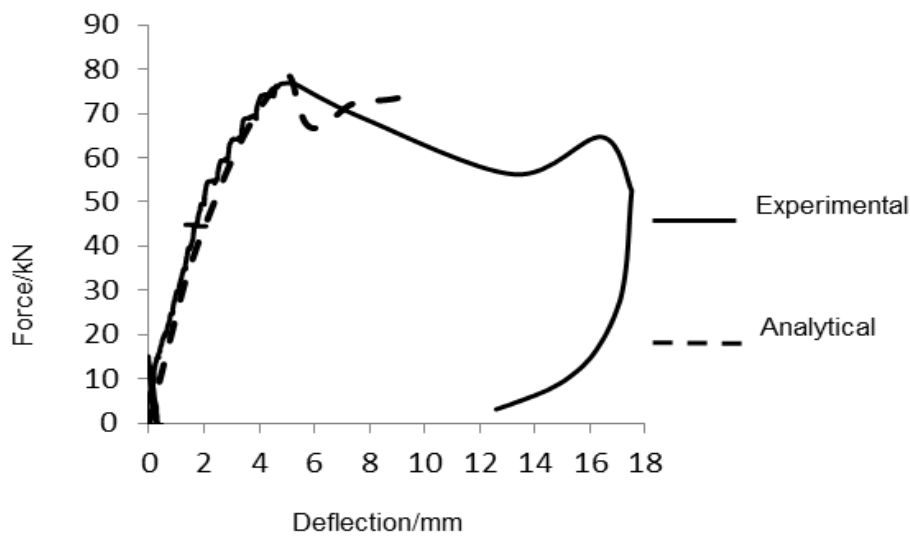


Figure 22. Load-deflection curve for Wall 7

5 Conclusion

In this research seven tests have been performed, four on single-leaf walls, and three on double-leaf walls (these being quite a rarity in existing literature), to evaluate the influence that a collar-jointed masonry addition can provide to the deformation and strength performance of an isolated masonry wall. Two variants for the retrofitting application were examined; either on a “fresh” single-leaf undamaged wall (i.e. quoted as pre-earthquake) or on a lightly damaged single-leaf wall (i.e. quoted as post-earthquake). Based on the results from the single-leaf walls, the mortar strength doesn’t have a remarkable influence on the mechanical behaviour of masonry walls as different types of mortar both result in a very similar failure pattern and failure load. Diagonal cracking was observed to be the main failure pattern in both the single-leaf and double-leaf masonry walls under the application of an external effectively diagonal loading. Compared to the single-leaf wall, the double-leaf masonry not only has a higher capacity and ductility, but also improves the integrity (reducing cracking and residual

stiffness). For the scenario where the collar joint technique was applied as a pre-earthquake enhancement method (discarding the differential aging parameter of the two masonry leafs) was found very effective in terms of failure load and stiffness increase. When used as post-earthquake retrofitting the technique was also quite effective particularly in terms of stiffness and ductility increase. The apparent additional options of considering different degrees of initial damage, parametrically altering the mortar parameters and modifying the mechanical bond of the two leafs should be seen as means of enriching this research which in this preliminary stage showed promising novel results.

Furthermore, a numerical micro-modelling approach has been carried out to validate the experimental findings. The results although the bold character of some parameter idealisation showed a relatively good agreement in aspects such as the ultimate load and stiffness while for most cases under-predicted the capacity for substantial plastic deformation, a feature which is critical in any earthquake related study where the hysteretic infill performance is critical in the holistic structural performance.

Acknowledgements

The authors would like to thank the China Scholarship Council (CSC) and the University of Leeds for providing the financial support of this project.

References

1. Mehrabi A, Shing BP, Schuller M, Noland J. Experimental evaluation of masonry-infilled RC frames. *Journal of Structural Engineering, ASCE* 1996; **122**(3):228-237.
2. Ehsani M, Saadatmanesh H, Velazquez-Dimas J. Behavior of retrofitted URM walls under simulated earthquake loading. *Journal of Composites for Construction, ASCE* 1999; **3**(3):134-142.
3. ElGawady MA, Lestuzzi P, Badoux M. A review of conventional seismic retrofitting techniques for URM. In: Proc 13th international brick and block masonry conference. 2004.
4. ElGawady MA, Lestuzzi P. A review of retrofitting of unreinforced masonry walls using composites. In: Proc 4th international conference on advanced composite materials in bridges and structures. 2004.

5. ElGawady MA, Lestuzzi P, Badoux M. Retrofitting of masonry walls using shotcrete. In: *NZSEE Conference*. 2006. No 45.
6. Bhattacharya S, Nayak S, Dutta SC. A critical review of retrofitting methods for unreinforced masonry structures. *International Journal of Disaster Risk Reduction* 2014; **7**:51-67.
7. Alcaino P, Santa-Maria H. Experimental response of externally retrofitted masonry walls subjected to shear loading. *Journal of Composites for Construction ASCE* 2008; **12**(5):489-498.
8. Mahmood H, Ingham JM. Diagonal compression testing of FRP-Retrofitted unreinforced clay brick masonry wall specimens. *Journal of Composites for Construction ASCE* 2011; **15**(5):810-820.
9. Anand SC, Yalamanchili KK. Three-dimensional failure analysis of composite masonry walls. *Journal of Structural Engineering ASCE* 1996; **122**(9):1031-1039.
10. Pina-Henriques J, Lourenco PB, Binda L, Anzani A. testing and modelling of multiple-leaf masonry walls under shear and compression. In: Modena C, Lourenco PB, Roca P, editors. Proceedings of the 4th international seminar on structural analysis of historical constructions, Balkema: Leiden (NL); 2004; 1: p.299-310.
11. Ramalho MA, Taliencio A, Anzani A, Binda L, Papa E. A numerical model for the description of the nonlinear behaviour of multi-leaf masonry walls. *Advances in Engineering Software*, 2008; **39**(4):249-257.
12. Binda L, Pina-Henriques J, Anzani A, Fontana A, Lourenco PB. A contribution for the understanding of load-transfer mechanisms in multi-leaf masonry walls: testing and modelling. *Engineering Structures* 2006; **28**(8):1132-1148.
13. British Standard Institution, BS 5628-1:2005. Code of practice for the use of masonry-Part 1: Structural use of unreinforced masonry.
14. Peraza D. Special problems with composite multiwythe masonry walls. *Forensic Engineering* 2009; 66-73.

15. Lourenco PB. Computations of historical masonry constructions. *Progress in Structural Engineering and Materials* 2002; **4**(3):301-19.
16. Chaimoon K, Attard MM. Modeling of unreinforced masonry walls under shear and compression. *Engineering Structures* 2007; **29**(9):2056-2068.
17. Page AW. Finite-Element Model for Masonry. *Journal of the Structural Division, ASCE* 1978; **104**(8):1267-1285.
18. Lourenco PB. Computational strategies for masonry structures. PhD thesis. Netherlands: Delft University of Technology; 1996.
19. Al-Chaar GL, Mehrabi A. 2008. Constitutive models for nonlinear finite element analysis of masonry prisms and infill walls (No. ERDC/CERL TR-08-19), US Army Corps of Engineering.
20. Van Zijl GPAG. Modelling masonry shear-compression: role of dilatancy highlighted. *Journal of Engineering Mechanics* 2004 **130**:1289-1296.
21. Dolatshahi KM, Aref AJ. Two-dimensional computational framework of meso-scale rigid and line interface elements for masonry structures. *Engineering Structures* 2011; **33**(12):3657-3667.
22. Cundall PA. A computer model for simulating progressive large scale movements in blocky rock systems. In: Proceedings of the symposium of the international society of rock mechanics, Nancy, France; 1971.
23. Lemos JV. Discrete element modelling of masonry structures. *International Journal of Architectural Heritage* 2007; **1**:190-213.
24. Sarhosis, V, Sheng, Y. Identification of material parameters for low bond strength masonry. *Engineering Structures* 2014; **60**:100-110.
25. Sarhosis, V, Garity SW, Sheng Y. Influence of brick-mortar interface on the mechanical behaviour of low bond strength masonry brickwork lintels. *Engineering Structures* 2015; **88**:1-11.
26. Midas FEA. Nonlinear FE Analysis Software. MIDAS Information Technology Co, (2013) CSP FEA.

27. British Standard Institution, BS 3921:1985. Specification for Clay bricks.
28. British Standard Institution, BS EN 772-1:2011, Methods of test for masonry units, Part 1: Determination of compressive strength.
29. British Standard Institution, BS EN 1015-11:1999, Methods of test for mortar for masonry-Part 11: Determination of flexural and compressive strength of hardened mortar.
30. Vermeltfoort AT, Raijmakers TMJ. Shear tests on masonry walls. In: Proc 6th North American masonry conference. 1993; p.1183-1193.
31. Van der Pluijm R. Material properties of masonry and its components under tension and shear. In: Proc 6th Canadian masonry symposium, Saskatchewan, Canada, 1992; p.675-686.
32. Ghaboussi J, Barbosa R. Three-dimensional discrete element method for granular materials. *International Journal for Numerical and Analytical Methods in Geomechanics* 1990 **14**:451-72.
33. Oliveira DVC. Experimental and numerical analysis of blocky masonry structures under cyclic loading. PhD thesis. Portugal: University of Minho; 2003